Meccanica (2008) 43: 349–363
DOI 10.1007/s11012-007-9101-7

Critical defect size distributions in concrete structures detected by the acoustic emission technique

A. Carpinteri · G. Lacidogna · G. Niccolini · S. Puzzi

Received: 24 October 2006 / Accepted: 15 June 2007 / Published online: 5 December 2007

Abstract Extensive research and studies on concrete fracture and failure have shown that concrete should be viewed as a quasi-brittle material having a size-dependent behavior. Numerous experimental techniques have been employed to evaluate fracture processes, and a number of modeling approaches have been developed to predict fracture behavior. A non-destructive method based on the *Acoustic Emission* (AE) technique has proved to be highly effective, especially to assess and measure the damage phenomena taking place inside a structure subjected to mechanical loading. In this paper, comparing AE frequency-magnitude statistics in solids subjected to damage processes with defect size distributions for disordered materials, critical parameters defining instability conditions for monitored structures are found. In addition, an experimental investigation conducted on concrete and RC structures by means of the AE technique is described. Experimental results confirm the described theories.

Keywords Defect size distribution · Acoustic emission · Concrete structures · Damage mechanics · Mechanics of solids and structures

A. Carpinteri (✉) · G. Lacidogna · G. Niccolini · S. Puzzi
Department of Structural Engineering & Geotechnics, Politecnico di Torino, Corso Duca degli Abruzzi 24, 10129 Torino, Italy
e-mail: alberto.carpinteri@polito.it

1 Introduction

The AE monitoring technique is similar to the one employed in earthquake control, where seismic waves reach the monitoring stations situated on the surface of the Earth. Though they take place on very different scales, these two families of phenomena—damage in structural materials and earthquakes in geophysics—are very similar: in either case, in fact, we have a release of elastic energy from sources located inside a medium. Characterizing the nature of AE sources is an open and discussed argument in the scientific literature. Researches have been conducted on this subject in the scientific community from the waveforms captured by the AE measurements systems. Though the acoustic emission technique can be used also to detect phenomena such as creep or shrinkage [1], here only AE caused by an active mechanical loading is considered. It produces a stress field which is further aggravated by defects causing the AE [2]. Accordingly, the AE technique can be an effective method for monitoring the integrity of large-sized structures, such as buildings, dams and bridges and other constructions, by means of a limited number of sensors.

Another similarity between complex seismic phenomena and damage processes in structures, as assessed by means of the AE, is provided by the statistical distribution of earthquakes quantified by the Gutenberg-Richter (GR) law [3]. By applying this law to AE analysis, it is also possible to obtain a statistical correlation between the number of AE events (N) and

signal amplitude during the structural damage process. Furthermore, in the analysis of these phenomena play the statistical and theoretical models of fracture mechanics a very important role. These models permit to find, through fractal laws, the critical exponents (scale-invariant) related to damaged materials. Such parameters identify the critical defect size distribution on all scales [4–8]. Indeed it is generally true that, where a critical phenomenon is imminent (e.g. material failure), not only the macroscopic defect size is relevant. Other defect or energy scales must be considered together with the macroscopic one. They are interacting to produce the macroscopic phenomenon. The AE permits to find the defect dimension through the detected released energy. By using these theories, we can gain a better understanding of the relationship between microstructural events and macroscopic behavior and we are in a better position to formulate predictive models, about either laboratory scale effects or full-size structural performance and reliability.

Studies on the role played by the different mechanism of failure in different situations can be performed, besides the AE waveform analysis, through the Moment Tensor Analysis. This is a tool successfully exported from Seismology to AE technique, which permits to determine orientations of cracks and crack types [26]. The authors are working on this subject which, however, has been well settled by Ohtsu in many international papers [9].

2 AE frequency-magnitude statistics

In AE monitoring, piezoelectric (PZT) sensors are used, thereby exploiting the capacity of certain crystals to produce electric signals whenever they are subjected to a mechanical stress. The adopted equipment in this investigation consists of many units USAM®, that can be synchronized for multi-channel data processing. Each unit contains a preamplified wideband resonant sensor sensitive at the frequency range between 50 kHz and 800 kHz.

Acoustic emission is defined as the energy released in the form of mechanical vibration from a material as it undergoes stress. Such stress generates deformation and fracture. The acoustic emission is an omni directional wave that travels from the source to the sensor via the material itself.

In this way, AE sensors can be employed as strainmeters, that is for an indirect measurement of strain, when used to evaluate the damage evolution in a structural element. In fact, the strain and the AE count generally increase in a proportional way.

If the AE sensors are actually employed to measure the propagation velocity of the ultrasonic signals generated by microfractures inside the material, then they work as accelerometers measuring changes in the wave-propagation velocity per unit time.

Resonant sensors were used, since concrete attenuates strongly the emissions and maximum sensitivity was required. The most relevant parameters acquired from the signals (arrival time, amplitude, duration, and number of oscillations) are stored in the USAMs memory and then downloaded to a PC for a multi-channel data processing.

Extracting some parameters from the AE waveforms is usually referred to as parameter-based AE technique. In Sect. 4, another kind of resonant sensor is described, which simply counts the occurrence of AE events. This procedure for signal processing is called event counting technique. Both kind of sensors filter out low frequency disturbances signals (below 50 kHz) coming from the environment. By means of the parameter-based technique microcracks localization can be performed and the condition of the specimen is determined, while event counting technique permits only zone location, where the general region of an AE source is determined.

Along the lines of the earthquake seismology [3], the magnitude in terms of AE technique is defined as follows:

$$m = \mathrm{Log}_{10} A_p + f(r), \tag{1}$$

where A_p is the signal amplitude, measured in microvolts, while $f(r)$ is a correction taking in account that the amplitude is a decreasing function of the distance r between the source and the sensor. According to Uomoto [10], for large-sized structures, the amplitude reduction factor for AE signals in concrete is $f(r) = kr$, where r is measured in meters and k is equal to five magnitudes per meter.

In seismology, earthquakes of larger magnitude occur less frequently than earthquakes of smaller magnitude. This fact can be quantified in terms of a magnitude-frequency relation, proposed by Gutenberg and Richter in an empirical way:

$$\mathrm{Log}_{10} N(\geq m) = a - bm, \quad \text{or} \quad N(\geq m) = 10^{a-bm}, \tag{2}$$

where N is the cumulative number of earthquakes with magnitude $\geq m$ in a specified area and over a specified time span, and b and a are positive constants varying from region to region [3, 11].

The GR relationship has been tested successfully in the acoustic emission field to study the scaling of the "amplitude distribution" of AE waves [7, 12–15]: this approach substantiates the similarity between the damage process in a structure and the seismic activity in a region of the Earth's crust and, at the same time, it widens the scope of the GR relationship. From (2), we find that the b-value is the negative gradient of the log-linear AE frequency-magnitude diagram and hence it represents the slope of the amplitude distribution. The b-value changes systematically with the different stages of fracture growth [7, 12–15], and hence it can be used to estimate the development of fracture process.

3 Damage size-scaling

3.1 The GR relation in geophysics and mechanics

The aim of the present section is to establish a theoretical basis for taking as the critical parameter $b_{\min} = 1$, as it being observed both in AE laboratory tests and in tests performed on full sized engineering structures [7, 13].

In order to give a reasonable characterization to the microcrack opening in a damaged material, the following similarity conditions are introduced, as already done in seismology for the faults [17, 18]:

$$w/L = c_1 = \text{const}, \qquad \bar{\delta}/L = c_2 = \text{const}, \tag{3}$$

where $\bar{\delta}$ is the relative displacement of the two lips of the fault, L and w (length and width) are the dimensions of the defect, whose area is thus $S = wL \sim L^2$.

Let us consider again the GR relation, written in the following form:

$$\text{Log}_{10}(N \geq m) \propto -bm. \tag{4}$$

Another relation between the magnitude of an AE event and L, valid in seismology for most common cases of earthquakes [17], is assumed:

$$m \propto 2\,\text{Log}_{10} L. \tag{5}$$

Taking into account (3), a comparison between (1) and (5) shows that the area of a microcrack is proportional to the corresponding AE amplitude, as confirmed by experimental results [19].

Furthermore, combining (4) and (5) gives:

$$\text{Log}_{10}(N \geq L) \propto \text{Log}_{10} L^{-2b}, \tag{6}$$

where N is the number of AE events generated by source microcracks advancements with a characteristic linear dimension $\geq L$.

Equation (6) can be rewritten as:

$$N(\geq L) = cL^{-2b}. \tag{7}$$

From (7) it results that the number of AE events generated by source defects with a characteristic linear dimension $\geq L$ follows a power law, where $2b$ is the scaling exponent of the length distribution and c is the total number of AE events. Therefore, the GR frequency-magnitude distribution is a power law with a fractal exponent $2b$ [20, 21]. See Turcotte [21], where the concept of seismic moment is recalled, for a more extended derivation of (7) or, alternatively, Aki [20], where basic concepts of fractal geometry are used.

3.2 Critical defect size distribution

In the framework of damage mechanics for disordered materials, such as concrete and rocks, the random distribution of microcracks existing in a body can be treated by a probability density function $p'(L, \vartheta, \varphi)$, L, ϑ and φ being respectively the size of defect, the latitude and the longitude of its orientation.

If ΔL, $\Delta\vartheta = (0, \pi)$, $\Delta\varphi = (0, 2\pi)$ are the ranges of microcracks parameters, the following relation holds by definition:

$$\int_0^{\Delta L} \mathrm{d}L \int_0^{2\pi} \mathrm{d}\varphi \int_0^{\pi} p'(L, \vartheta, \varphi) \sin\vartheta \,\mathrm{d}\vartheta = 1. \tag{8}$$

When in a disordered material it is reasonable to assume an isotropic distribution of microcracks, the probability density will take the form:

$$p'(L, \vartheta, \varphi) = \frac{p(L)}{4\pi}, \tag{9}$$

$p(L)$ being the probability density of size distribution, so that:

$$\int_0^{\Delta L} p(L)\mathrm{d}L = 1. \tag{10}$$

Now, let us consider a body of characteristic linear size s; we can compute the value $\bar{L}$ of the crack size, such that, on average, one defect only (i.e. the largest) exceeds it. Let the cracking in the body be uniform over a fractal domain of dimension $2 \leq D \leq 3$, so that we may define ρ as the mean fractal density of defects. Hence, the following relation holds:

$$1 = \Pr[L \geq \bar{L}]\rho s^D \int_{4\pi} \frac{\mathrm{d}\Omega}{4\pi}, \tag{11}$$

where $\mathrm{d}\Omega \equiv \sin\vartheta\,\mathrm{d}\vartheta\,\mathrm{d}\varphi$ is the element of the solid angle surrounding the direction (φ, ϑ). Integrations over ϕ and ϑ (i.e. over the solid angle of 4π sr subtended by a unit sphere) have been carried out since L can have any orientation.

It is of interest the particular size distribution $p(L)$ for which the maximum defect size $L_{\max}$ in a body is proportional to the linear size s of the body itself, $L_{\max} \propto s^{\delta}$, the condition $\delta = 1$ representing the case of perfect self-similarity, which is illustrated in Fig. 1(c), whereas, in general, δ can be different from 1, entailing simply self-affinity (see Fig. 2).

Assuming this hypothesis if a geometrically similar body of characteristic size ks is considered (k is thus a dimensionless size ratio), we impose that only one defect only exceeds the threshold $k^{\delta}\bar{L}$; it is thus possible to write:

$$1 = \Pr[L \geq k^{\delta}\bar{L}]\rho(ks)^D \int_{4\pi} \frac{\mathrm{d}\Omega}{4\pi}. \tag{12}$$

Equating the right-hand terms of (11) and (12) we readily obtain:

$$\Pr[L \geq k^{\delta}\bar{L}]k^D = \Pr[L \geq \bar{L}]. \tag{13}$$

The solution of (13) is [4–7]:

$$P(L) = 1 - \frac{c_0}{\gamma L^{\gamma}}, \quad \forall L > L_0, \tag{14}$$

with:

$$\gamma = \frac{D}{\delta}, \tag{15}$$

where c_0 is a constant of proportionality and L_0 is an upper limit for the intrinsic defects of the body. By derivation of P, which gives the probability to find a defect with size $\leq L$, we obtain the following probability density function:

$$p(L) = \frac{c_0}{L^{\gamma+1}}, \quad \forall L > L_0. \tag{16}$$

It can be observed that $L_{\max}$ is, in a body of size ks, a random value exceeding the threshold $k^{\delta}\bar{L}$, and now we also know that L is distributed according to the probability function of (16), which will be referred to as the defect size distribution of self-affinity. The number of defects with size $\geq L$ expected from the distribution of (14) or (16) is [7]:

$$N(\geq L) \propto L^{-\gamma}. \tag{17}$$

The cumulative distribution of (17) is formally identical to the GR cumulative distribution of (7). Therefore, if we now consider the defects as sources of AE activity, we can equate distributions (7) and (17), obtaining [7]:

$$\gamma = 2b. \tag{18}$$

From the literature on AE tests, it is well-known that the b-value decreases as the body approaches impending failure [7, 12, 13]. It is common to observe a trend of b to the critical value $b_{\mathrm{crit}} = 1$ during final crack propagation [7, 13]. In order to explain this experimental evidence, we exploit properties of the distribution of self-affinity given by (16) [7]. Substituting (18) into (15) we obtain the following expression for b:

$$b = \frac{D}{2\delta}. \tag{19}$$

The minimum of the b-value is obtained when $D = 2$ and $\delta = 1$ and it is thus equal to 1.

In order to prove this, we note that the scaling relation of self-affinity, $L_{\max} \propto s^{\delta}$, is equivalent to the following relations:

$$s(k) \propto k, \tag{20}$$

$$L_{\max}(k) \propto k^{\delta}, \tag{21}$$

where k is the previously introduced dimensionless scaling factor.

From (20) and (21) in the case $\delta > 1$, the largest defect (or crack) results to be larger than the body itself for sufficiently large scales (see Fig. 3), suggesting a complete separation of the body. This paradox sets to 1 the upper limit to the values of δ, and then it theoretically accounts for $b_{\mathrm{crit}} = 1$ as a lower limit to the b-values commonly observed in AE monitoring tests on specimens loaded up to the failure. In fact, the conditions $D = 2$, which is a lower limit reached when

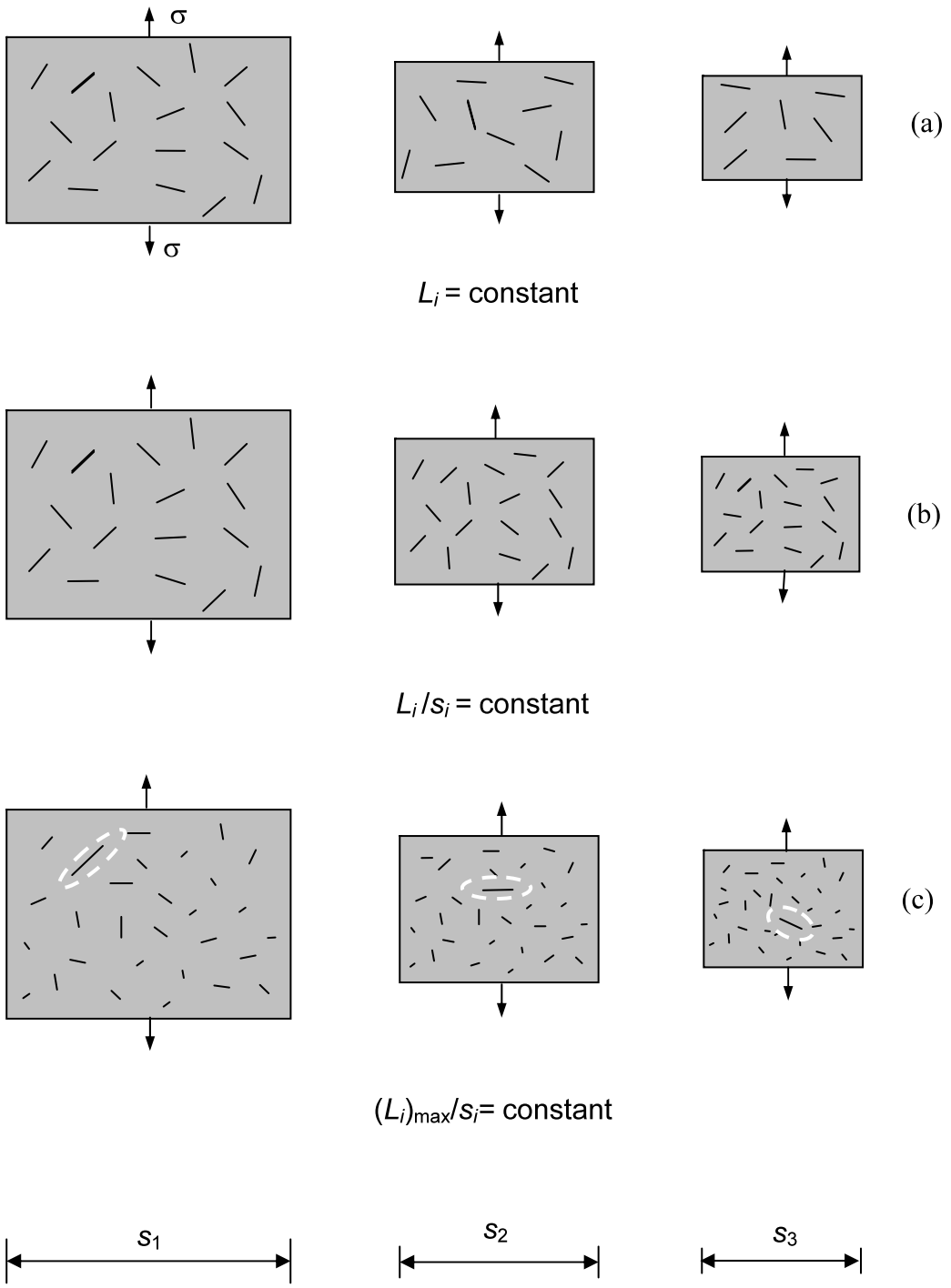

Fig. 1 Geometrically similar bodies with many random defects: constant defect size (**a**); defect size constant and proportional to the body size (**b**); defect size distribution of self-similarity (**c**) [2]

damage concentrates over the through-going fracture surface, and $\delta = 1$, i.e. the maximum defect assumed to be proportional to the characteristic size of the body, are both reached at the collapse [7].

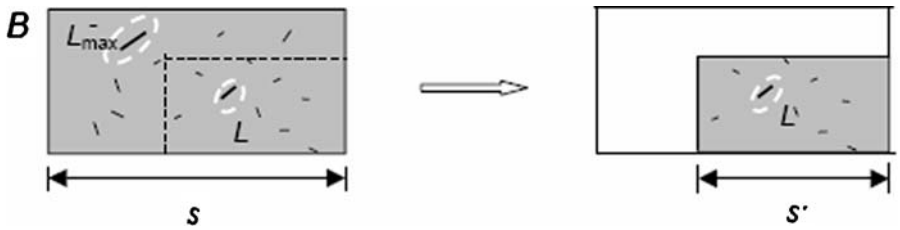

Fig. 2 In a portion k times smaller than the body B, the size L of its largest defect is statistically given by solving the equation $k^{\delta} = L/L_{\max}$

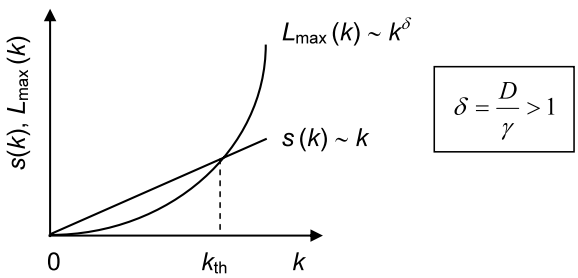

Fig. 3 Trends of body size s and maximum defect size $L_{\max}$ as functions of the scale in the case of defect size distribution with $\delta > 1$. This plot accounts for $\delta = 1$ as an upper limit to the values of δ. For suitably small scales ($k < k_{\text{th}}$) defect size distributions with $\delta > 1$ have physical meaning

Till now no particular assumption has been made about γ, which in principle may take any value >1. In reality, values smaller than 2 should not be allowed, since b usually doesn't drop below 1 (see (18)). Nevertheless, for suitably small values of k, i.e. for sufficiently small bodies, defect size distributions with $1 < \gamma < 2$ have physical meaning, since the inequality:

$$L_{\max}(k) < s(k), \tag{22}$$

can be still satisfied even if $\delta > 1$, see Fig. 3. In fact, loosing the limit condition $\delta = 1$ implies that γ can be smaller than 2, in accordance with (15).

In terms of b-value, the condition $1 < \gamma < 2$ reads:

$$1/2 < b < 1. \tag{23}$$

Experimental results confirm the possibility that the b-value reaches values comprised between $1/2$ and 1, which can be explained in terms of power-law defect size distributions [12–15, 26].

An AE monitoring test may last beyond the critical limit of a structure. In fact, after breaking into smaller parts, a body may be held together because of either boundary conditions or structural characteristics. For example, triaxial tests, realized superimposing a confining pressure on a uniaxial stress, are common on rocks in order to simulate the conditions found in Earth's crust. A compressive fracture occurs by a shear fault along an inclined plane in a specimen held together by the imposed confining pressure. The changes in the b-values with time show a minimum as cracks interact to form an inclined shear fault (Fig. 4) [12].

Another example is cracking in a reinforced concrete beam subjected to cyclic load, which finally leads to breaking into several parts held together by steel reinforcement (Fig. 5) [13].

That would thus result in splitting the initial one-body system in a multi-body system, characterized by reduced scaling factors k', k'', k''', etc. (see Fig. 5). Scaling reduction below a threshold k_{th} makes meaningful distributions with $1 < \gamma < 2$ (see Fig. 3), corresponding to observed b-values between $1/2$ and 1.

It is possible therefore to conclude that usually $\gamma = 2$ is a lower limit for power-law defect size distributions [4–7], from pre-critical to critical conditions, in agreement with the minimum values $b_{\min} = 1$ observed experimentally both in AE laboratory tests and in tests performed on full sized engineering structures [7]. It is worth noting that b-values in the range $(1/2, 1)$ have been observed in Tectonics as well [21, 26]. An explanation of these values in terms of defect size distributions leads to a *post-critical regime*, which regulates bodies under particular conditions. The fragmentation of a structure into a multi-body system seems to reproduce, on strongly reduced scale, the outline proposed by the Theory of Plate Tectonics, where the Earth's surface is broken into large plates moving against each other (Fig. 6) [21, 26].

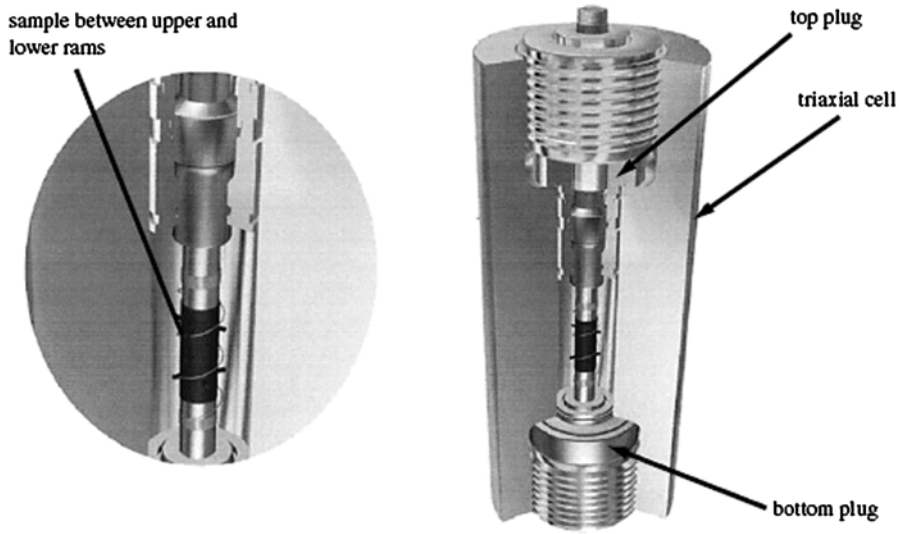

(a)

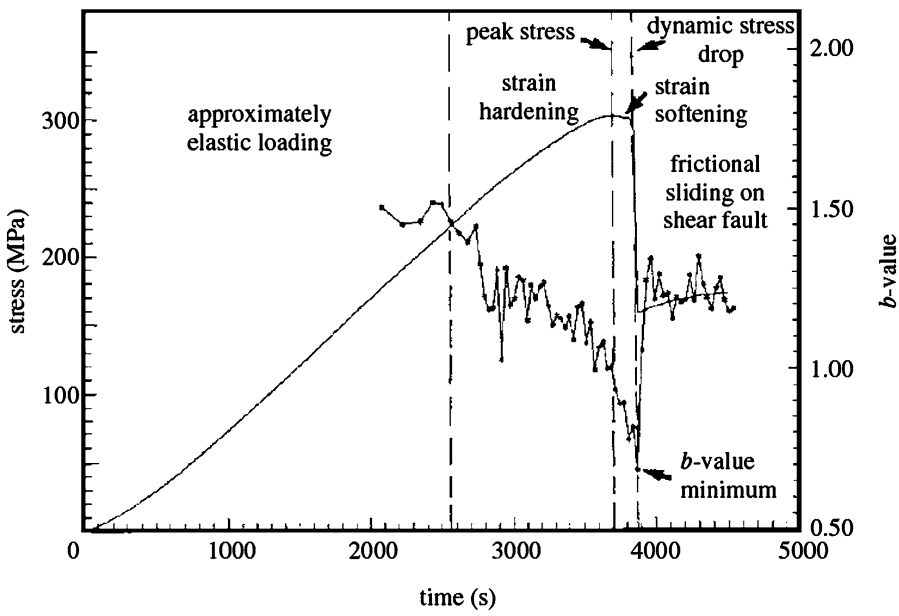

(b)

Fig. 4 Triaxial experiment for rock deformation. **a** Triaxial testing cell. The rock sample is jacketed in a multiple-instrumented plastic sleeve to keep out the confining fluid. **b** Triaxial deformation experiment on air-dried sandstone at 50 MPa confining pressure. Acoustic emissions are measured concurrently with deformation. The *b*-value exhibits a single minimum (reprinted from [12])

The *b*-value analysis emphasizes the analogy between these two multi-body systems, since in both cases *b*-values smaller than 1 can be observed. In Tectonics, it has been shown that the *b*-value varies systematically for different modes of faulting [26].

4 Calculation of AE energy

Besides the magnitude and the seismic moment, the third important characteristic is the measured energy of a single AE event. The total energy W released by an AE event is estimated by Harris et al. [27],

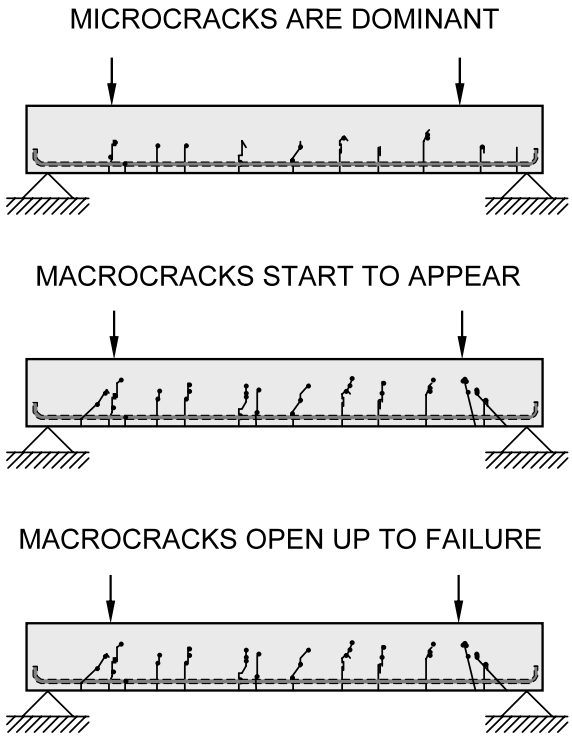

Fig. 5 Fracture process developments during different stages of loading. *Dotted line* outlines steel reinforcement (reprinted from [13])

$$W = \frac{1}{R}\sum_{i=1}^{n}\int_0^{\Delta t_i} A_i(t)^2 \mathrm{d}t, \tag{24}$$

where $A_i(t)$ is the output voltage of the sensor S_i, Δt_i is the event duration, i.e., the time from the first to the last threshold crossing of the signal $A_i(t)$, R is the resistance of the measuring circuit, and the sum is extended over all the n detecting sensors.

In order to calculate the integrals in (24), a decaying sinusoid for the voltage is assumed [19]:

$$A_i(t) = A_{p,i}\sin(2\pi f t)\exp(-t/\tau), \tag{25}$$

where $A_{p,i}$ is the signal amplitude, τ is the decay constant, and f is the signal frequency.

The energy is related to the magnitude by the second GR relation [3, 21]:

$$\mathrm{Log}_{10} W = c_0 m + d_0, \quad \text{or} \quad W \propto 10^{c_0 m}. \tag{26}$$

Obtaining AE information according to the above-discussed theoretical approach needs a quite sophisticated data acquisition and analysis system. Therefore, in long-term tests, such as creep tests, the recording and interpretation of gigabytes of data becomes a practical limitation.

A second approach, which uses less sophisticated hardware and software to perform acquisition and calculation, is the ring-down counting. Such approach is simply counting the number of times n_0 the threshold voltage A_{th} is exceeded over a determined time window by the oscillating transducer output. The whole burst of oscillations in each time window are counted as one event. Although some features of the original AE signal are sacrificed, this method preserves some weighting in favor of events of larger energy, and an estimation of the energy released W_j in one AE event j is given by the ring-down count n_{0j} [28, 29]:

$$W_j \propto n_{0j}. \tag{27}$$

In the framework of damage mechanics an internal variable called *damage parameter* η was defined to measure the accumulated state of damage in a material [4, 30, 31]. The damage variable η is related by definition to the total area of the cracks and can be analyzed in terms of acoustic emissions through the following relation [32]:

$$\eta \equiv K\sum_j L_j^2 \propto \sum_j 10^{m_j}, \tag{28}$$

where m_j is the magnitude of the AE event j, the sum is extended over all detected events [29], and K is a renormalization constant.

Equation (27) can be linked to (5), which says that the magnitude is proportional to the logarithm of source rupture area.

The total ring-down count N for the test is given by the sum of the partial ring-down counts n_{0j} over all the time windows:

$$N = \sum_j n_{0j} \propto \sum_j W_j \propto \sum_j 10^{c_0 m_j} \propto \sum_j L_j^{2c_0}, \tag{29}$$

where (26–28) and (5) are inserted.

Since the last summation is extended over a myriad of damage microsurfaces for which the usual concepts of Euclidean geometry may no longer be appropriate, (29) seems to be consistent with the following fractal scaling law:

$$N \propto W \propto V^{D/3}, \tag{30}$$

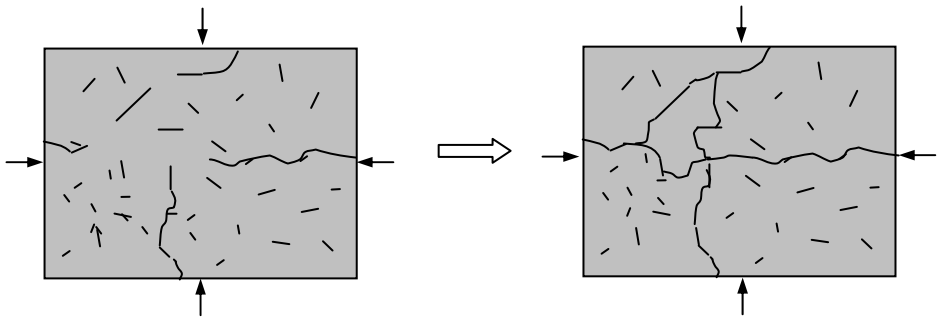

(a)

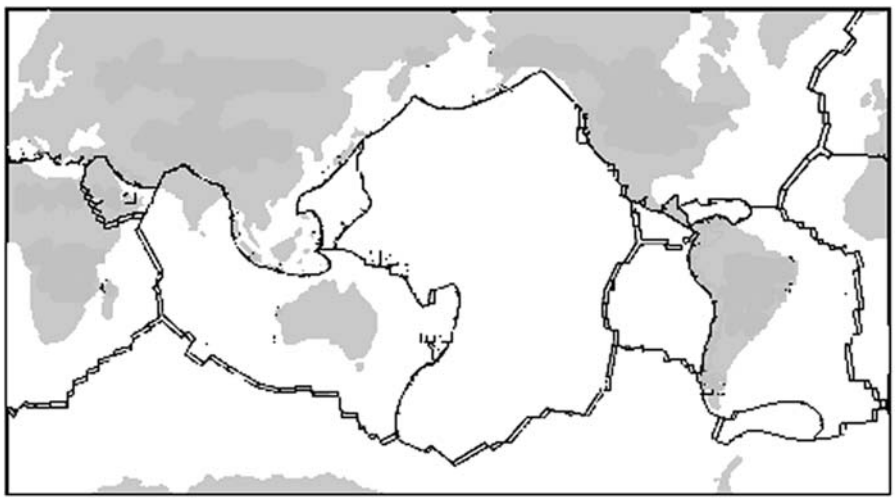

(b)

Fig. 6 Similarity in fragmentation of a structure into multi-body system on different scales, from laboratory specimen (**a**) to Earth's crust (**b**)

where V is the specimen volume, W is the total released energy by AE, and D is the dimension of the fractal domain whence AE energy radiates. Equation (30), which is referred to as fractal scaling law, takes into account the principles on the energy dissipation also shown by other researchers [22–25], and derives from experimental observations carried out by the authors from the scale of laboratory specimens (with size $\sim$ cm) to the full-size structures ($\sim$m), both on quasi-brittle materials (i.e. concrete) and composite materials (i.e. masonry). This equation is valid for prediction of stability conditions of structures with size ranging over several orders of magnitude, and in particular for large structures, and the fractal exponent D turns out to be comprised between 2 and 3, showing that damage takes place in a fractal domain comprised between a surface and a volume [29].

Besides the released energy, through the ring-down counting it is possible also to estimate the b-value of the GR law.

An estimation b^* of the b-value is obtained by formally applying the GR distribution (see (2)) to the ring-down count in a specified time window (here the subscript j is omitted for the sake of simplicity):

$$\begin{aligned} &\mathrm{Log}_{10}\, n(\geq m_0) = a^* - b^* m_0, \quad \text{or} \\ &n(\geq A_0) = 10^{a^*} A_0^{-b^*}, \end{aligned} \tag{31}$$

where: $m_0 \equiv \mathrm{Log}_{10}\, A_0$.

Identifying A_0 with the threshold voltage A_{th}, (31) is used to find an expression for the number n_0 of the ring-downs counted in a specified time window:

$$n_0 \equiv n(\geq A_{\text{th}}) = \int_{A_{th}}^{\infty} \left| \frac{\mathrm{d}n}{\mathrm{d}A_0} \right| \mathrm{d}A_0$$

$$= 10^{a^*} b^* \int_{A_{\text{th}}}^{\infty} \frac{\mathrm{d}A_0}{A_0^{b^*+1}} = \frac{10^{a^*}}{A_{\text{th}}^{b^*}}. \tag{32}$$

The parameter a^* is obtained by formally setting $A_{\text{th}} = 1$ μV; in this case the ring-down count saturates, and (31) takes the form:

$$\text{Log}_{10} n_{\text{MAX}} = a^* - \text{Log}_{10} 1 = a^*, \tag{33}$$

where n_{MAX} is the counting capacity of the transducers. Inserting (33) in (32) gives:

$$n_0 = \frac{n_{\text{MAX}}}{A_{\text{th}}^{b^*}}. \tag{34}$$

Solving (34) with respect to b^* gives:

$$b^* = \frac{\text{Log}_{10} n_{\text{MAX}} - \text{Log}_{10} n_0}{\text{Log}_{10} A_{\text{th}}}. \tag{35}$$

Therefore, the b^*-value is a sort of saturation index of the counting capability of the transducers, and it depends on the adopted transducers and the fixed threshold. Low values of b^* correspond to high values of n_0 indicating a large amount of AE activity, i.e. a large damage amount, whereas high values of b^* correspond to low values of n_0 indicating a small amount of AE activity, i.e. a small damage amount. In this sense b^* offers an estimation of the b-value.

When AE Atel® equipment is adopted [29, 33], considering a threshold level of $A_{\text{th}} = 100$ μV, the oscillation counting limit is fixed at 255 oscillations every 120 s. With this equipment $n_{\text{MAX}} = n \times 255$ is obtained, where n is a positive integer defining the time window amplitude during the monitoring.

In this case the b^*-value is given by:

$$b^* = \frac{1}{2}[\text{Log}_{10}(n255) - \text{Log}_{10} n_0], \tag{36}$$

where n_0 is the number of ring-downs counted during a time window of $n \times 120$ s.

5 Damage time-scaling

The authors have also shown that energy release W, as measured with the AE technique during the damaging process, follows this *time-scaling* law [7]:

$$W(t) \propto N(t) \propto t^{\beta_t}, \tag{37}$$

where t is the monitoring time, N is the total number of AE events relating to a certain predetermined magnitude, m_0, and taking place over a certain time period, and β_t stands for the time-scaling exponent of the released energy.

Equation (37) describes—as Omori's law does [11], but in simpler, more intuitive terms—the sequences of foreshocks and aftershocks characterizing the failure of a structural member during a loading test. In effect, power laws similar to (37) for the temporal evolution of AE rate, including the Omori's law, drawn without considering the geometry of the structures are largely present in the literature [34, 35]. By working out the β_t exponent from the data obtained during each observation period, we can make a prediction as to the stability of a structure. If $\beta_t < 1$, the damaging process slows down, because energy dissipation tends to decrease; if $\beta_t > 1$ the process becomes unstable, and if $\beta_t \cong 1$ the process is metastable, i.e., though it evolves linearly over time, it can reach either stability or instability conditions indifferently. By introducing (2) into (37) we get the experimental relationship between the b-value of the GR law and the time-scaling exponent β_t:

$$N(\geq m_0, t) = 10^{a(t) - b(t) m_0} \propto t^{\beta_t}. \tag{38}$$

During the application of the load to a structural member, whether on a laboratory or a full size scale, the critical condition (mainshock) can be identified as the condition in which AE signal amplitude is greatest. Accordingly, from (38) it is possible to determine the $a(t)$, $b(t)$ time-dependent coefficients and the β_t parameter for each interval in the time succession analysed. In general, we find that in the sequences of signals preceding the critical condition (foreshock) $\beta_t > 1$, and in those that follow (aftershock) $\beta_t < 1$. The parameter b, on the other hand, in keeping with experimental observations [7, 13], and theoretical predictions [4–7], decreases continuously until it reaches its critical value $b_{\text{min}} = 1$ when the structure reaches the collapse condition.

6 Experimental observations

6.1 In situ retrofitted RC beam test

Utilizing the AE technique, we have monitored and analysed a retrofitted RC beam with non-rectangular

cross-section (Fig. 7). To improve its load carrying capacity and attenuate the effects of microcracking, the beam was externally reinforced with FRP sheets after the prior removal of the existing overload [33]. Then, an *in-situ* loading test of the retrofitted beam was carried out.

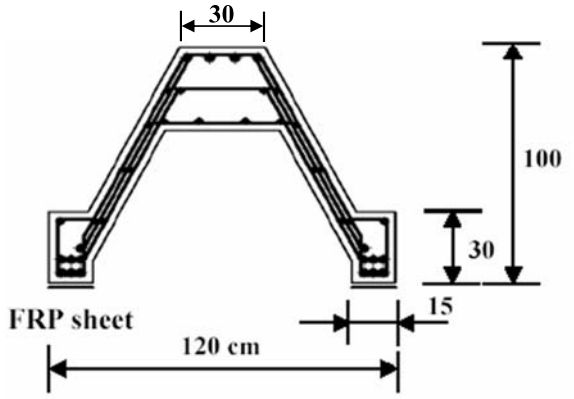

Fig. 7 *In situ* retrofitted RC beam test. Scheme of the beam cross-section

The entire loading test lasted approximately 3 hours. During the test, five transducers (S_i) were applied to one of the lateral faces of the beam. The AE source points were determined and are shown in Fig. 8(b) with black dots. In the loading range considered, micro-slips between the FRP sheets and concrete were not high enough to cause delamination. AE transducers, in fact, detected the onset of debonding only. The time evolution of the AE counting numbers, as detected by the AE transducers, is shown in Fig. 8(c). Transducers 3 and 4 were close to flexural cracks and began to detect AE events from the beginning of the loading test. At the end of the test, they had detected the highest number of AE, followed by transducers 1 and 2, which were close to the beam supports.

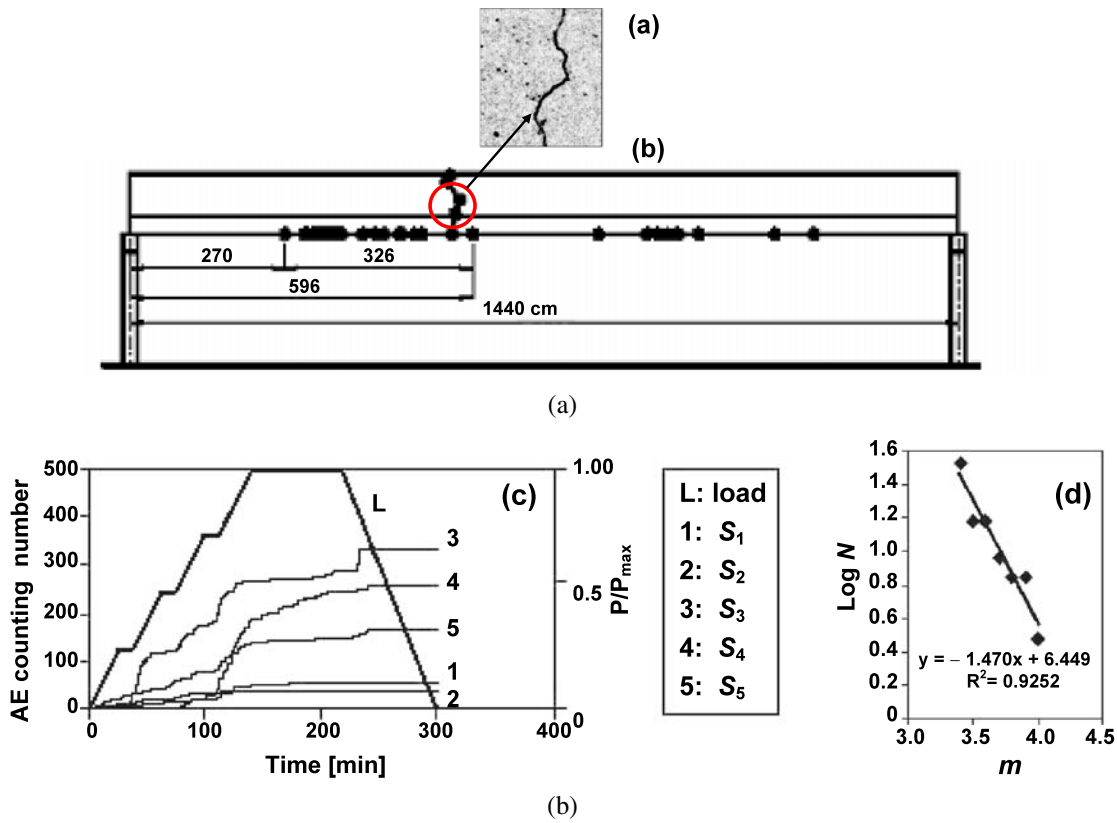

Fig. 8 *In situ* retrofitted RC beam test. **a** Photo of a flexural crack in between transducers 3 and 4 (using an optical microscopy with magnification 100X). **b** Scheme of the beam indicating localized AE sources. **c** AE counting number for each sensor S_i during the loading test. **d** *b*-value during the loading test

This result is in agreement with the typical progression of cracking and collapse in retrofitted beams. Flexural cracks propagate upwards as loading progresses, but remain very narrow throughout the loading history. Delamination of the FRP sheets together with a thin layer of concrete takes place only when shear cracks develop in the proximity of the supports.

In addition to the crack localization, the cumulative number of AE events with magnitudes greater than m, as a function of m, was plotted on a semi-logarithmic scale. The final determination for the magnitude of an AE event is based on the average value of the results recorded by all the sensors. The reading of a single sensor is found using (1). From Fig. 8(d) a good agreement with the GR relationship is observed: the b-value is approximately equal to 1.47.

6.2 Three-point bending test

The behavior of a specimen subject to a three-point bending test was investigated. To determine the fracture process zone, AE generation was monitored. The specimen was a prism measuring $8 \times 15 \times 70$ cm^3, with a central 5 cm notch cut into it beforehand to ensure a central crack. Five AE transducers were fitted to the specimen at points shown in Fig. 9(a). During the loading test, the source location procedure was successfully applied to identify the fracture process zone, as shown in Fig. 9(a). Nucleation in the fracture process zone might be correlated with the AE clusters zone, and AE clusters are seen to propagate with increasing load [33, 36, 37]. The load vs. time curve for the specimen, characterizing the AE activity, is shown in Fig. 9(b). In order to assess the ability of the AE technique to monitor the microscopic damages occurring inside the material and obtain information about the fracture processes, the load-time diagram, plotted for each second of the testing period, was broken down into three stages: a first stage (t_0, t_1) extending from the initial time to peak load, a second stage (t_1, t_2) going from peak load to the peak of AE activity, or mainshock [13–15] , and a third stage (t_2, t_f) going from the mainshock to the end of the process. In accordance with the GR law, b-values are shown for each stage in Fig. 9(c). In this case too the b-values are seen to be in good agreement with the GR law: they range from 1.49 to 1.11. The minimum value is obtained in the softening branch of the load-time curve, and it is very close to 1, as suggested in [7, 13].

6.3 Concrete specimen in compression

Laboratory tests also analysed the behavior of cylindrical concrete specimens in compression [21]. One of the 59 mm diameter specimens, with a height/diameter ratio $h/d = 2$, is shown in Fig. 10(a). The compression test was performed in displacement control, by imposing a constant rate of displacement to the upper loading platen. A displacement rate equal to 4×10^{-4} mm/s was adopted to obtain a very slow crack growth. The role of driving rate has been analysed in a recent study on scaling characteristics of fracture in rocks [38] and apparently it doesn't influence the evolution of the b-value. Compressive load vs. time, cumulated event number, and event rate (for each second of the testing period) are reported in Fig. 10(b). Also in this case, the load vs. time diagram was subdivided into three stages. The b-values obtained for each stage are shown in Fig. 10(c); they range from 1.63 to 1.19. The minimum value, close to 1, was again obtained in the softening branch of the load vs. time curve. Finally, for the three loading stages, Fig. 10(d) gives the values of the β_t parameter. The values, between 1.62 and 0.58, were determined by best fitting the cumulating count of the AE events divided by the total count for each loading stage. These results confirm that, during the sequence of signals preceding the critical condition (foreshock), $\beta_t > 1$, whereas, during the sequence following the critical condition (aftershock), $\beta_t < 1$, energy dissipation being exhausted. It should be noted that a comparative reading of b-value and β_t parameter makes it possible to assess the evolution of the entire damage process: β_t defines the rate of damage growth, whereas b defines the current state of damage. β_t parameters, in fact, have a *predictive* function relative to the reaching of the critical condition, whereas b-values have a *descriptive* function relative to the damage level reached.

7 Conclusion

The acoustic emission (AE) technique has the potential for performing an effective monitoring of the integrity of large-sized structures, such as Civil Engineering structures, by means of a limited number of sensors. By applying the AE technique to structural members monitored during the damaging process, a statistical correlation between the number of AE

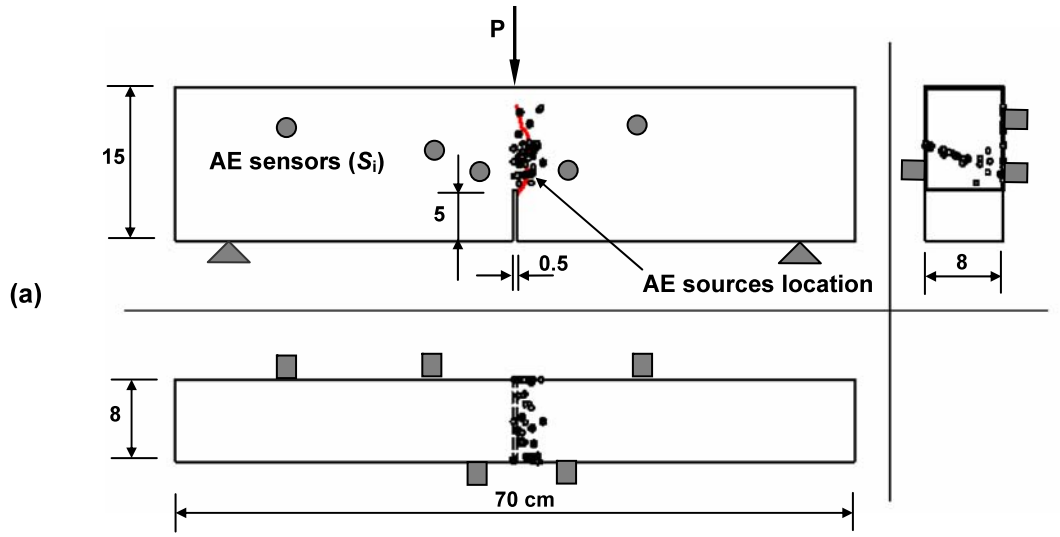

(a)

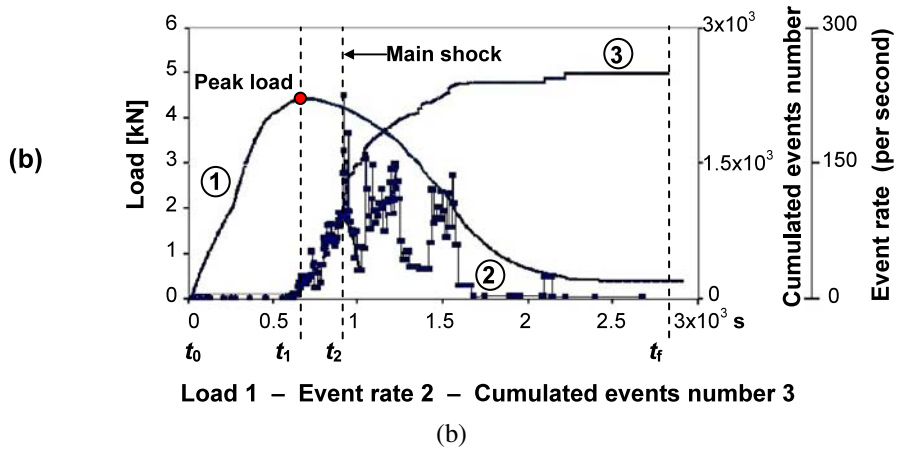

(b)

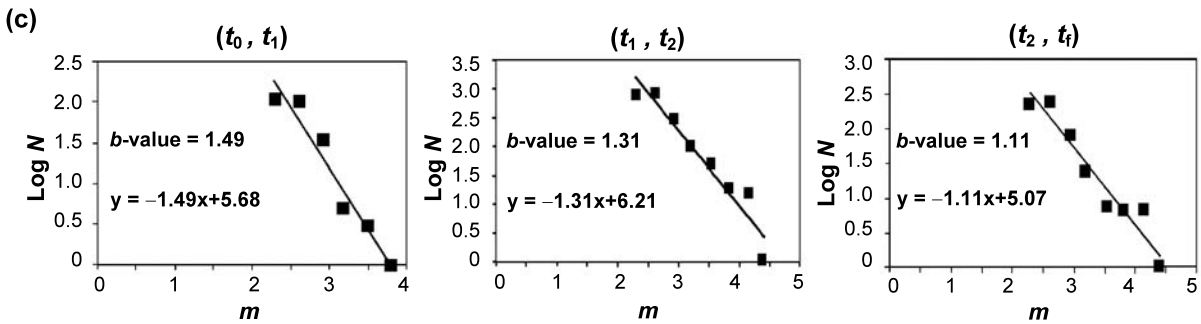

Fig. 9 Three bending point test. **a** Identification of the fracture process zone. **b** Load vs. time curve and AE activity. **c** *b*-values during the loading test

events and their amplitude was established by quantifying the *b*-value for each loading stage; at the same time, the time-scaling was determined through the β_t parameter. Moreover, by utilizing the statistical models of damage mechanics, it has been possible to propose a theoretical explanation of the lower limit of the

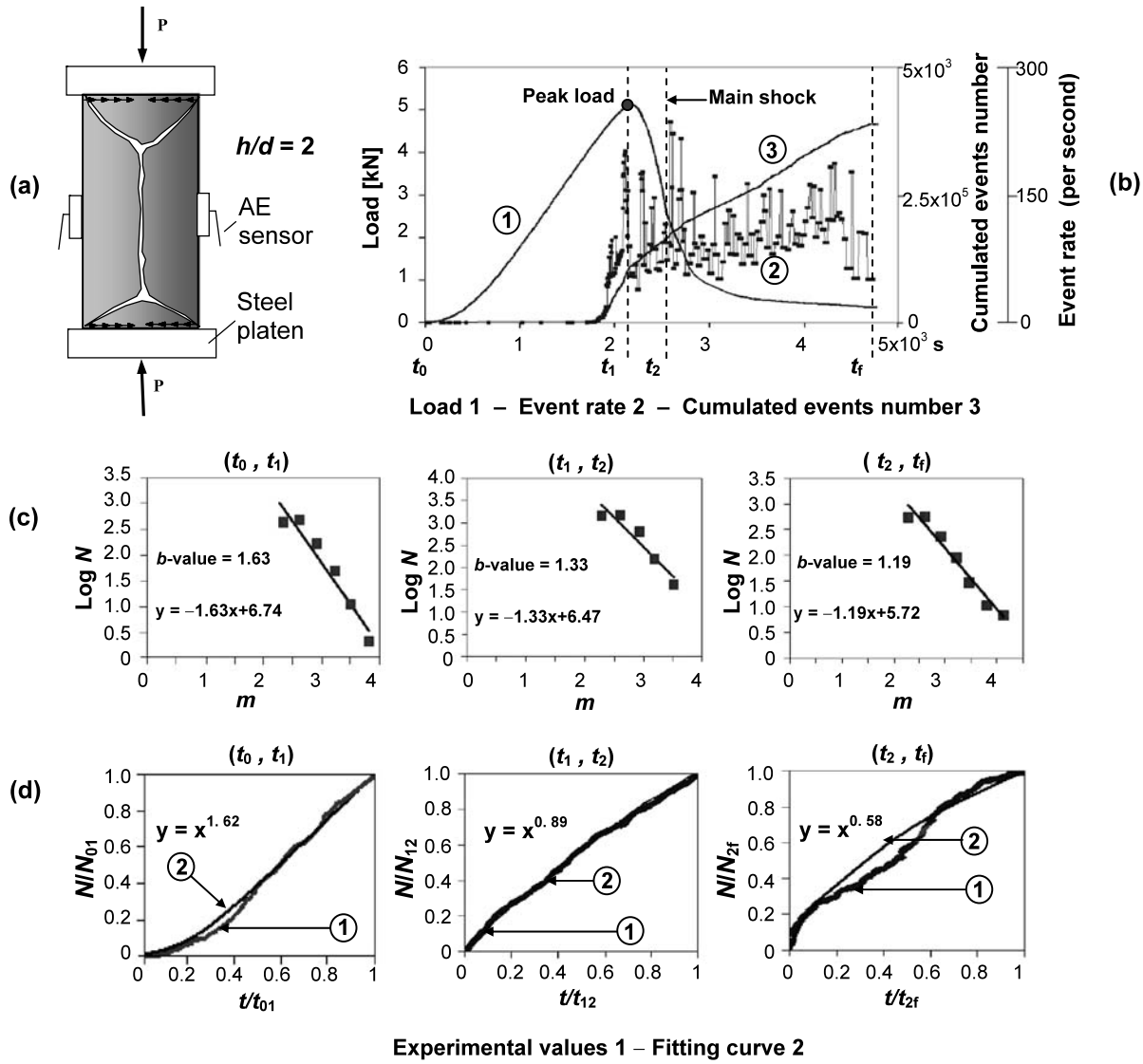

Fig. 10 Cylindrical concrete specimen in compression. **a** Testing set-up. **b** Load vs. time curve and AE activity. **c** *b*-values during the loading test. **d** Variation in β_t parameter during the test

b-value characterizing the critical defects size distribution emerging at the structural collapse. From the values of these two coefficients we can get a better understanding of the relationship between microstructural events and macroscopic behavior and we are in a better position to formulate predictive models, about either laboratory scale-effects or full-size structural performance and reliability.

Acknowledgements Support of the Ministry of University and Scientific Research (MIUR) and of the European Union (EU) is gratefully acknowledged. The authors would like to thank Prof. Alessandro Pellizzola for very helpful suggestions and valuable discussions.

References

1. Rossi P, Godart N, Robert JL, Gervais JP, Bruhat D (1994) Investigation of the basic creep by acoustic emission. Mater Struct 27:510–514
2. Pollock AA (1968) Stress wave emission—a new tool for industry. Ultrasonics 6:88–92
3. Richter CF (1958) Elementary seismology. Freeman, New York

4. Carpinteri A (1986) Mechanical damage and crack growth in concrete: plastic collapse to brittle fracture. Nijhoff, Dordrecht
5. Carpinteri A (1989) Decrease of apparent tensile and bending strength with specimen size: two different explanations based on fracture mechanics. Int J Solids Struct 25:407–429
6. Carpinteri A (1994) Scaling laws and renormalization groups for strength and toughness of disordered materials. Int J Solids Struct 31:291–302
7. Carpinteri A, Lacidogna G, Niccolini G (2006) Critical behavior in concrete structures and damage localization by acoustic emission. Key Eng Mater 312:305–310
8. Carpinteri A, Lacidogna G, Pugno N (2006) Richter's laws at the lab-scale interpreted by acoustic emission. Mag Concr Res 58:619–625
9. Ohtsu M, Okamoto T, Yuyama S (1998) Moment tensor analysis of acoustic emission for cracking mechanisms in concrete. ACI Struct J 95:87–95
10. Uomoto T (1987) Application of acoustic emission to the field of concrete engineering. J Acoust Emiss 6:137–144
11. Rundle JB, Turcotte DL, Shcherbakov R, Klein W, Sammis C (2003) Statistical physics approach to understanding the multiscale dynamics of earthquake fault systems. Rev Geophys 41:1–30
12. Sammonds PR, Meredith PG, Murrel SAF, Main IG (1994) Modelling the damage evolution in rock containing porefluid by acoustic emission. In: Proceedings of Eurock'94, Rotterdam
13. Colombo S, Main IG, Forde MC (2003) Assessing damage of reinforced concrete beam using "*b*-value" analysis of acoustic emission signals. J Mater Civ Eng ASCE 15:280–286
14. Kapiris PG, Balasis GT, Kopanas JA, Antonopoulos GN, Peratzakis AS, Eftaxias KA (2004) Scaling similarities of multiple fracturing of solid materials. Nonlinear Process Geophys 11:137–151
15. Ojala IO, Main IG, Ngwenya BT (2004) Strain rate and temperature dependence of Omori law scaling constants of AE data: implications for earthquake foreshock-aftershock sequences. Geophys Res Lett 31:1–5
16. Burridge R, Knopoff L (1964) Body force equivalents for seismic dislocations. Bull Seismol Soc Am 54:1875–1888
17. Kanamori H, Anderson DL (1975) Theoretical basis of some empirical relations in seismology. Bull Seismol Soc Am 65:1073–1096
18. Scholz CH (2005) The scaling of geological faults. In: Proceedings of the 11th international conference on fracture (ICF11), Turin
19. Pollock AA (1973) Acoustic emission, 2: acoustic emission amplitudes. Non-Destr Test 6:264–269
20. Aki K, Richards PG (1980) Quantitative seismology: theory and methods. Freeman, New York
21. Turcotte DL (1997) Fractals and chaos in geology and geophysics. Cambridge University Press, Cambridge
22. Karihaloo BL (1999) Size effect in shallow and deep notched quasi-brittle structures. Int J Fract 95:379–390
23. Barenblatt GI (2005) Scaling phenomena in fatigue and fracture. In: Opening lecture at the 11th international conference on fracture, Turin
24. Morel S, Schmittbuhl J, Bouchaud E, Valentin G (2000) Scaling of crack surfaces and implications for fracture mechanics. Phys Rev Lett 85:1678–1681
25. Weiss J (2001) Self-affinity of fracture surfaces and implications on a possible size effect on fracture energy. Int J Fract 109:365–381
26. Schorlemmer D, Wiemer S, Wyss M (2005) Variations in earthquake-size distribution across different stress regimes. Nature 348:539–542
27. Harris DO, Tetelman AS, Darwish FA (1972) Detection of fiber cracking by acoustic emission. In: Liptai RG, Harris DO, Tatro CA (eds) Acoustic emission, STP505. American Society for Testing and Materials, Philadelphia
28. Brindley BJ, Holt J, Palmer IG (1973) Acoustic emission, 3: the use of ring-down counting. Non-Destr Test 6:299–306
29. Carpinteri A, Lacidogna G, Pugno N (2007) Structural damage diagnosis and life-time assessment by acoustic emission monitoring. Eng Fract Mech 74:279–289
30. Lemaitre J, Chaboche JL (1990) Mechanics of solid materials. Cambridge University Press, Cambridge
31. Krajcinovic D (1996) Damage mechanics. Elsevier, Amsterdam
32. Cox SJD, Meredith PG (1993) Microcrack formation and material softening in rock measured by monitoring acoustic emission. Int J Rock Mech Min Sci Geomech Abstr 30(1):11–21
33. Carpinteri A, Lacidogna G, Paggi M (2007) Acoustic emission monitoring and numerical modeling of FRP delamination in RC beams with non-rectangular cross-section. Mater Struct 40:553–566
34. Shcherbakov R, Turcotte DL (2003) Damage and self-similarity in fracture. Theor Appl Fract Mech 39:245–258
35. Turcotte DL, Newman WI, Shcherbakov R (2003) Micro and macroscopic models of rock fracture. Geophys J Int 152:718–728
36. Shah SP, Li Z (1994) Localisation of microcracking in concrete under uniaxial tension. ACI Mater J 91:372–381
37. Ohtsu M (1996) The history and development of acoustic emission in concrete engineering. Mag Concr Res 48:321–330
38. Kuksenko V, Tomilin N, Chmel A (2005) The role of driving rate in scaling characteristics of rock fracture. J Stat Mech: Theory Exp (electronic journal). doi:10.1088/1742-5468/2005/06/P06012